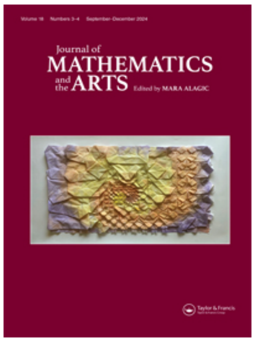

Journal of Mathematics and the Arts

ISSN: (Print) (Online) Journal homepage: www.tandfonline.com/journals/tmaa20

Floating mandalas

E. Farcot

JOURNAL OF MATHEMATICS AND THE ARTS
https://doi.org/10.1080/17513472.2025.2457917

Taylor & Francis
Taylor & Francis Group

OPEN ACCESS Check for updates

Floating mandalas

E. Farcot

School of Mathematical Sciences, University of Nottingham, Nottingham, UK

ABSTRACT

This article considers geometric patterns arising from infinite series of concentric circles, whose radii converge to zero. As an archetype of such design, the initial focus is on level curves of the surface given by $z = \sin(1/r)$ in cylindrical polar coordinates, before generalizing to other periodic functions. Since any horizontal section of this surface comprises an infinite number of circles, there is no physical medium on which a complete visualization can be achieved. As we explore different computer-based representations, the reader will be presented with a sample of surprisingly stunning patterns involving intricate arrangements of moiré and related patterns. Especially when considering rectangular grid approximations, these patterns are reminiscent of mandala figures. We discuss how they arise due to the finite nature of any computing or display device, epitomized by floating-point approximations of real numbers. Code is provided as a means to generate an endless supply of artworks.

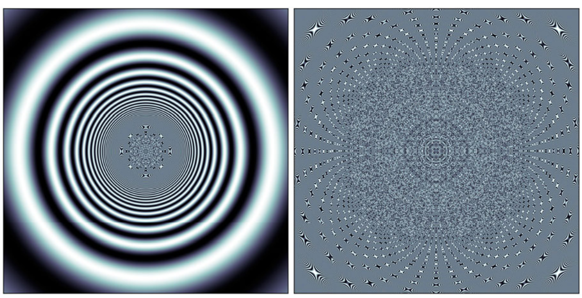

ARTICLE HISTORY
Received 29 November 2023
Accepted 21 January 2025

KEYWORDS
Topologist's sine curve; computer graphics; floating numbers; moiré patterns; mandalas

1. Introduction

The present paper explores patterns such as those seen in Figure 1, which represents a translated form of the topologist's sine curve $\sin(1/x)$, well known to mathematics undergraduates. As we apply this infinitely bending function to $\sqrt{x^2+y^2}$, we generate a surface comprising infinite concentric circular waves. Since these level curves consist of infinitely

CONTACT E. Farcot etienne.farcot@nottingham.ac.uk School of Mathematical Sciences, University of Nottingham, NG7 2RD, Nottingham, UK

Supplemental data for this article can be accessed online at http://dx.doi.org/10.1080/17513472.2025.2457917.

This article has been corrected with minor changes. These changes do not impact the academic content of the article.

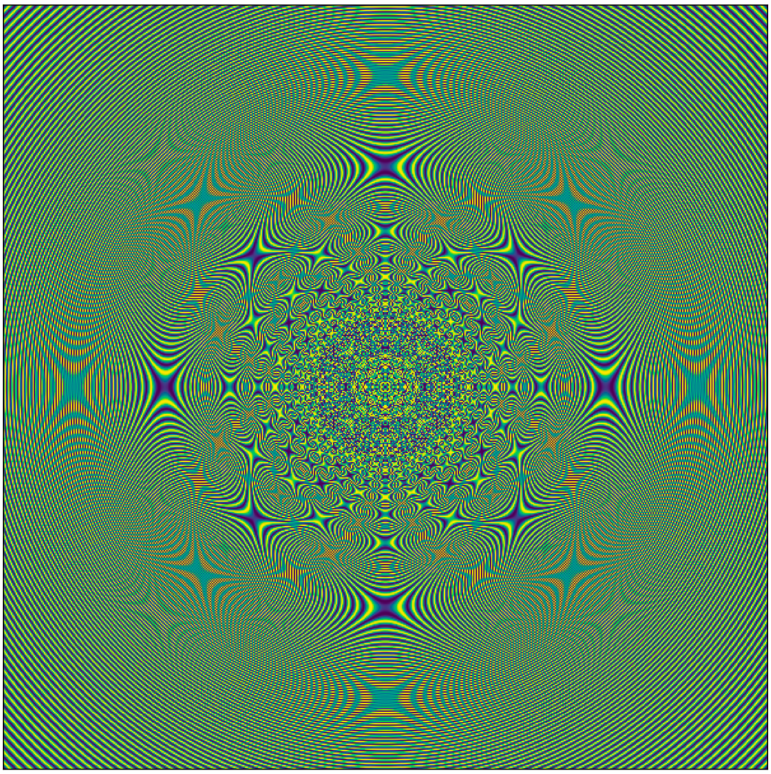

Figure 1. 'Heatmap' of the function $S(1/\sqrt{x^2+y^2})$ where $S(x) = \frac{(1+\sin(2\pi x/T))}{2}$ with $T = 0.01$, using a 600×600 grid of values x, y in the interval $[-1, 1]$. Each pixel is given a colour representing the value of the function using an colourmap, i.e. an interval of RGB values; see Section 4 for more details and alternative colourmaps. Generated using the command `imshow` from the matplotlib library (Hunter, 2007) with default options. The colourmap is the perceptually uniform `viridis`. Note that the appearance of the figure will vary depending on factors including the PDF viewing software, screen resolution or printing device.

many concentric circles, no computer representation, nor in fact the use of any physical medium, is able to represent this surface in its entirety. As a result of the approximation using a grid of floating number, it appears in Figure 1 that intricate combinations of random looking fluctuations appear, interwoven with classical moiré patterns (Amidror, 2009). These figures are strongly reminiscent of patterns presented in a previous publication (Kaplan, 2005) and references therein, as discussed in the following section. The remainder of this paper aims to provide some partial explanations to the patterns which are being observed. It will turn out that these are to a large extent unpredictable, being dependent upon fine details of the representation algorithm being used, and the device or material being used for display. We produce a sample of patterns and figures, which can all be created using very simple code instructions. The effect of varying different parameters, both mathematical and those underlying visualization algorithms, is explored on a selection of examples. It appears that the method provides an endless supply of artworks. All code is provided with the paper for readers wishing to promptly produce their own pieces of art, using examples in the paper as initial guide.

2. Mathematical background

In this section, we present a mathematical model underlying the different figures which will be presented subsequently. Besides providing some notations, in defining this model we will find that the key ingredients are the combination of a periodic function, composed with another which diverges at the origin. The exact nature of the periodic function will turn out to be of little consequence; the fact that is periodic is the most important factor as far as generating figures is concerned.

As a generic notation, we consider a real-valued function of the form

$$f(x) = S\left(\frac{1}{x^q}\right), \tag{1}$$

where $x > 0$, $q > 0$ is a steepness parameter and S is periodic of period $T > 0$. Assuming S (i.e. f) bounded, we set $0 \leqslant f(x) \leqslant 1$ without loss of generality. Then the main focus in this note are 2D patterns obtained by assigning colours to a grid of pixels using a function

$$f(r) = f(\|(x, y)\|). \tag{2}$$

Specifically, one will use different colourmaps, i.e. the assignment of a colour (typically RGB) for each possible value taken by f. As is often done, we call such 2d representations of (2) 'heatmaps'. Although commonly reserved for the Euclidean norm, the notation r will on occasion be abused to denote the ℓ^p norm for some $p \geqslant 1$. This extends to dependent terms such as 'circle', to be understood as a closed curve $\|(x - x_c, y - y_c)\| = \beta$, for some constant $\beta > 0$.

As mentioned, closely related patterns have been previously discussed (Kaplan, 2005); they were based on functions of the form (1) but with $q < 0$. A number of the points discussed below would still apply to these patterns, but 'in reverse': in the present case, the generating oscillation increases its frequency as one approaches the origin, whereas this happens away from the origin in said reference. As an addition to the discussion in this previous work, which focuses on aliasing, one will see here that the theory of moiré patterns provides further clarity on the nature of these patterns.

Since S is T-periodic, the level curves of the surface (2) are concentric circles, with radii given by the relation, valid for all $n \in \mathbb{N} = \{0, 1, 2, \dots\}$

$$\frac{1}{r_n^q} = \frac{1}{r_0^q} + nT \iff r_n^q = \frac{r_0^q}{1 + nTr_0^q} \implies f(r_0) = f(r_n). \tag{3}$$

Hence, any choice of r_0 generates a sequence of decreasing radii $\{r_n\}_n$. By periodicity of S it suffices to choose $1/r_0^q$ over the range $(0, T]$, i.e. r_0^q over $[\frac{1}{T}, \infty)$ to generate the complete surface specified by (2).

Remark 2.1: We introduce here a normalization convention. Any visualization of the level curves for f will have to be restricted to a bounded region within the plane. Let us agree on systematically using a square domain centred at the origin, say $(x, y) \in [-\alpha, \alpha]^2$. Then, rescaling it to $[-1, 1]^2$ by considering $(\tilde{x}, \tilde{y}) \doteq (x/\alpha, y/\alpha)$, one has that $\tilde{r} = \|(\tilde{x}, \tilde{y})\| = r/\alpha$ for any norm. Hence, $f(\tilde{r}) = S(\frac{\alpha^q}{r^q})$. Noting that concentric circles of same height are given by the relation

$$\frac{1}{r_{n+1}^q} - \frac{1}{r_n^q} = T \iff \frac{\alpha^q}{r_{n+1}^q} - \frac{\alpha^q}{r_n^q} = \frac{1}{\tilde{r}_{n+1}^q} - \frac{1}{\tilde{r}_n^q} = \alpha^q T,$$

it appears that it is equivalent to consider $0 < r \leqslant \alpha$ with a period T or $0 < \tilde{r} \leqslant 1$ with a period $\alpha^q T$. Therefore, every figure in this paper will be defined on the square $[-1, 1]^2$ (for which axes labelling will typically be omitted) without loss of generality, using T as main control parameter.

To obtain a representation which is independent of T we use a scaling parameter $\sigma \in (0, 1]$ such that (3) gives r_n in a simple form:

$$r_0^q = r_0^q(\sigma) = \frac{1}{\sigma T} \implies r_n^q = r_n^q(\sigma) = \frac{1}{(n+\sigma)T}. \tag{4}$$

As σ ranges over $(0, 1]$, (4) shows that for all natural numbers n, $r_n^q(\sigma)$ ranges over $I_n \doteq [\frac{1}{(n+1)T}, \frac{1}{nT})$, where for $n = 0$ the upper bound is understood as ∞. From this property, the punctured plane $\mathbb{R}^2 \setminus \{(0, 0)\}$ is indeed fully covered by a partition into annular regions $r \in I_n$. Any given circle $r = (r_0(\sigma))^{1/q}$, for $r_0 \in I_0$ has the same level as all $r_n(\sigma)$, for any other n. In equation, for any given σ one has a set of circles with a shared level and its simplest expression is $S(\sigma T)$:

$$f(r_n(\sigma)) = f\left(\frac{1}{(n+\sigma T)^{1/q}}\right) = S((n+\sigma)T) = S(\sigma T) = f(r_0(\sigma)).$$

The discussion above, including the expression for radii r_n given in (4), is independent of the exact form of the function S as long as it is T-periodic. Different choices of S will not affect the location of level curves, but only their height. In particular, while circles corresponding to a given σ always have the same level $S(\sigma T)$, the converse is only true if the restriction $\hat{S}$ of S to its fundamental interval $(0, T]$ is injective. We illustrate this fact in Figure 2, featuring two graphs of the form $S(1/r^2)$, where S is 2-periodic. One is a trigonometric function for which each $\alpha \in (0, 1]$ has two pre-images in the fundamental domain while the other, a saw wave function, is injective on $(0, T]$.

Since two-dimensional representations such as Figure 1 are the main focus of this note, the choice of S will effectively yield a device to associate colours to the concentric circles discussed above, whose location is exclusively dictated by the period T. In more formal terms, all figures presented in the remainder will be meant to represent a finite sample of the infinite family of circles $C(\sigma, n) \doteq \{(x, y) \mid r = (r_n(\sigma)\}$. A colour scheme in the present context is naturally described as a function from $[0, 1]$ to a three-dimensional colourspace, typically RGB values normalized between 0 and 1. Denote such a colour scheme by $\gamma : [0, 1] \to [0, 1]^3$. Then, all circles $C(n, \sigma)$ share the same colour $\gamma\,(S(\sigma T))$. As mentioned, if $\hat{S}$ is non-injective there will be several values of σ for which $S(\sigma T)$ is equal, and thus these circles will be assigned the same colour $\gamma\,(S(\sigma T))$. Since, in general, the colour scheme γ itself may be non-injective (for instance to a colourblind observer), one may argue that the fundamental structure underlying a visualization of the surfaces of the form (2) is that of circles $C(\sigma, n)$, which are independent of S. Given these circles, the function S can be

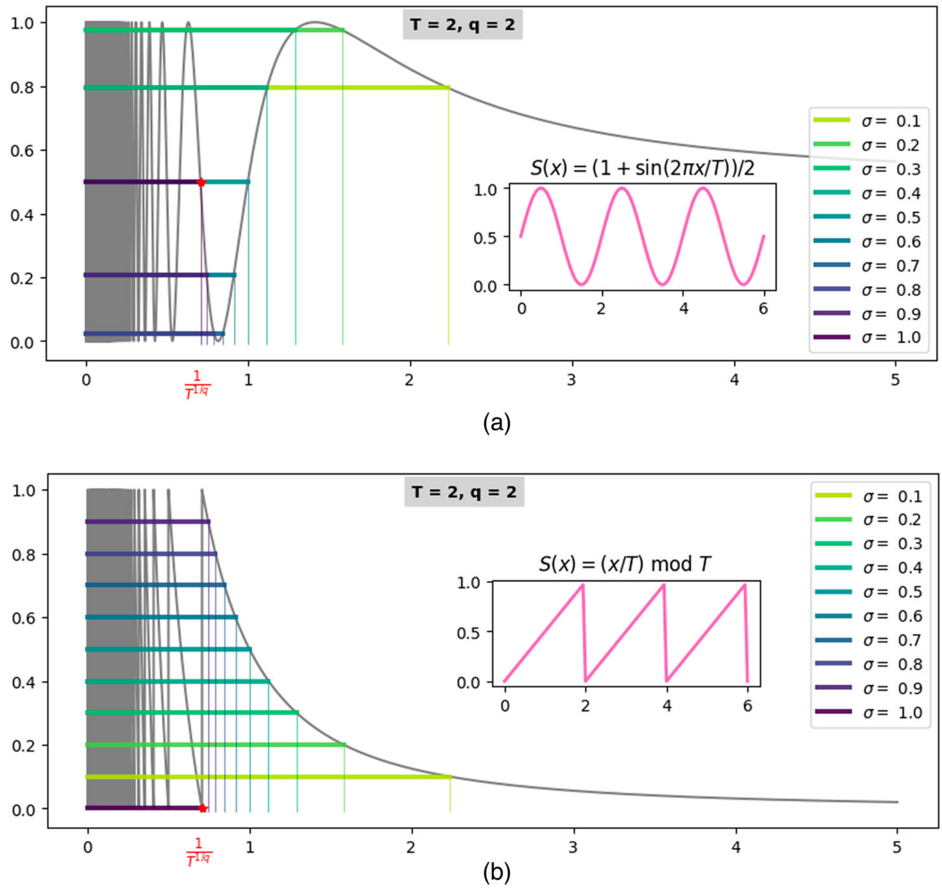

Figure 2. Two choices of periodic functions, represented with a sample of initial radii parameterized by $\sigma \in (0, 1]$. Each horizontal line has an infinite number of intersections with the graph of $S(1/r^q)$, at abscissas $r_n(\sigma), n \in \mathbb{N}$, see (4). In (a), the function S is non injective in $(0, T]$, so that two values of σ actually yield the same level curve. In contrast, in (b) injectivity ensures that each level $f(r) = z$ corresponds to unique family of circles $\{r = r_n(\sigma) : n \in \mathbb{N}\}$. (a) Section profile of $S(1/r^2), r > 0$ for a trigonometric $S(x)$, as shown in the insert. As σ varies, r_0 ranges over $[1/\sqrt{T}, \infty) = [1/\sqrt{2}, \infty)$. (b) Section profile of $S(1/r^2), r > 0$ for a saw wave $S(x)$, as shown in the insert. As σ varies, r_0 ranges over $[1/\sqrt{T}, \infty) = [1/\sqrt{2}, \infty)$.

thought of as a notational device to concisely encode the colour associated to each circle, in cases where γ is linear (or perceptually uniform Kovesi, 2015). In some instances, one will consider complex colourmaps, looking for aesthetic outcome rather than a precise mathematical control of the object being depicted; in such cases the choice of S will become largely irrelevant (though not without effect).

3. Practical implementation

Given the previous section, it is clear that the patterns visible in Figure 1 are artefacts; a correct figure should only include concentric circles. Since there are infinitely many of these circles, it is also clear that any method, be it on a computer or an analogue device,

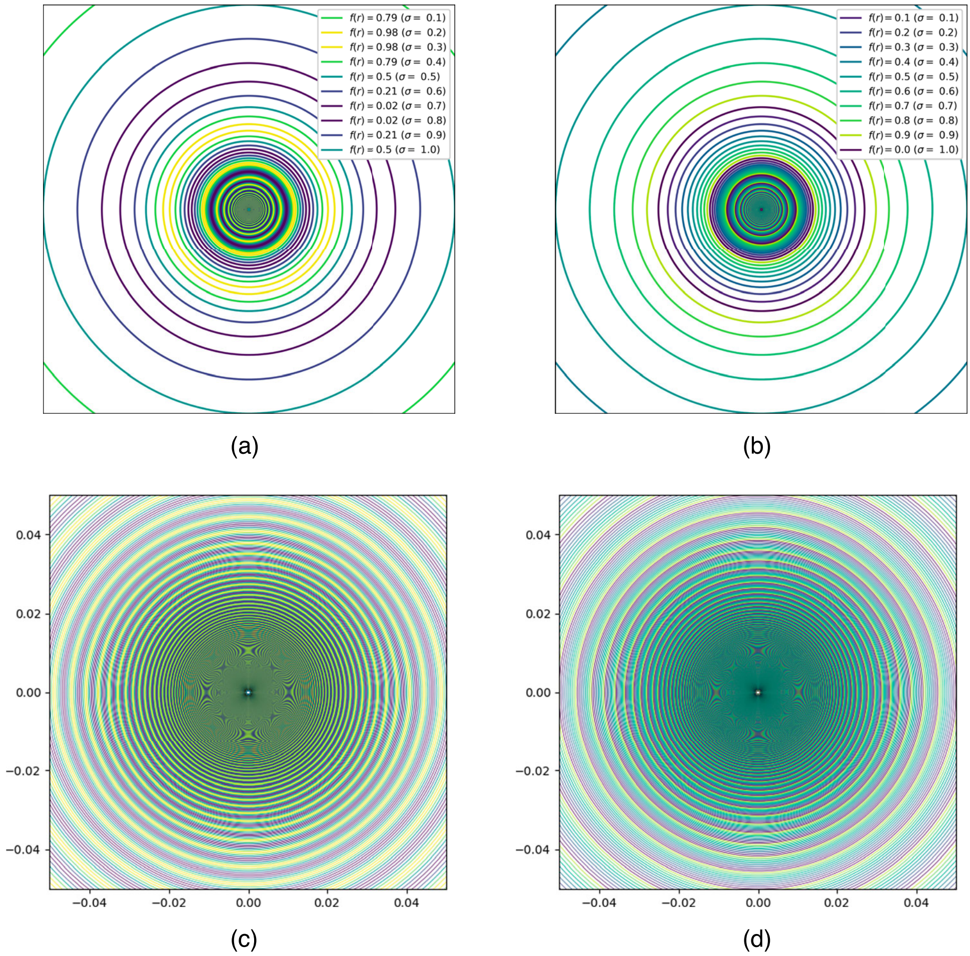

Figure 3. Level curves $f(r_n) = \alpha$, where S is 2-periodic, r_n as in (4), for $0 \leqslant n < 150$ and σ as shown in legend. The values of σ are exactly as in Figure 2, but colours are according to the height α. The non-injectivity in (a) leads to pairs of σ's yielding the same level, whereas each σ is associated with a single colour in (b). Depending on the device used to display this figure (especially, on print vs. digital), moiré patterns may be discerned near the origin, see zoomed-in versions in panels (c) and (d), where the range for n has been increased to $\{0 \dots 1000\}$. (a) Level curves for the trigonometric function shown in Figure 2(a). (b) Level curves for the saw wave function shown in Figure 2(b). (c) Zoom of panel (a). (d) Zoom of panel (b).

will only provide a finite approximation. An attempt at reducing the artefacts in Figure 1 is shown in Figure 3. The same two functions and σ values as in Figure 2 are used, now representing circles instead of a one-dimensional section. There are various methods to represent circles on a digital device (Blinn, 1987; Foley et al., 1995). In the figure, we use the `patches.Circle` method from the Matplotlib library, in Python (Hunter, 2007). The underlying algorithm builds a spline approximation of the circle. Further to this, by default the actual display relies on a number of modifiable methods to assign colour values to each pixel. For instance, anti-aliasing is performed by default, whereby colour intensity along a curve is distributed among the pixels it intersects according to the size of the overlap, rather than as Boolean assignment (Foley et al., 1995). In a later section, we will consider the visual effects of some display algorithms.

Using default settings as in Figure 3, moiré patterns are visible near the origin. Their hyperbola shape resembles patterns seen in the heatmap from Figure 1. This can be explained using classic techniques in moiré patterns theory, namely using the approach sometimes termed strain analysis (Amidror, 2009; Theocaris, 1969). In general, moiré shapes become visible when two or more repetitive patterns are superimposed. When these repetitive patterns are periodic, Fourier techniques provide powerful descriptive tool (Amidror, 2009). However in our case, even though in Figure 1 the patterns partly result from the digitized (x, y) grid of pixels, which is periodic, the series of concentric circles described in the previous section are not periodic. Indeed, the distance between a pair of successive radii $r_n(\sigma)$ is given by

$$r_n^q(\sigma) - r_{n+1}^q(\sigma) = \frac{1}{(n+\sigma)T} - \frac{1}{(n+1+\sigma)T} = \frac{1}{(n+\sigma)(n+1+\sigma)T}, \tag{5}$$

which depends on both n and σ.

Instead of Fourier methods, with strain analysis one explicitly describes the superimposed patterns, usually termed *gratings* in the literature, as level curve equations

$$f(x,y) = n, \quad g(x,y) = k,$$

where n, k range over some integer values. Then visible patterns can be understood as series of nearest intersection points, as long as no tangencies between gratings occur, such nearest point series are given by the two statements

$$n \pm k = \alpha,$$

for a constant α, as illustrated in Figure 4. Which of the two series of intersections is visible depends on the shape of 'parallelograms', formed by pairs of curves from each grating. This turns out to be amenable to elementary vector calculus, with the property that

$$n \pm k = \alpha \quad \text{is visible if} \quad \pm \nabla f \cdot \nabla g < 0, \tag{6}$$

as discussed in general references on moiré patterns (Amidror, 2009; Theocaris, 1969) or more specific work related to the present discussion (Cullen, 1990).

This is best visualized using an explicit example. In our case, regardless of whether one uses a heatmap or concentric circles, one conceives the displaying medium as composed of pixels. Hence, there are three underlying gratings: the horizontal and vertical lines lying between pixels in the pixel grid, and the concentric circles. Let ε designate the pixel size, assuming pixels are perfect squares. Then we denote the gratings using integer indices, k, l, n:

$$x_k = k\varepsilon, \quad y_l = l\varepsilon, \quad \text{and} \quad r_n(\sigma) = \frac{1}{(n+\sigma)T} \iff \frac{1}{Tr_n} - \sigma = n. \tag{7}$$

Then, from (6) we deduce that:

- Expectedly, patterns $k \pm l$, which arise within the x, y grid alone, are never visible since in that case using (6) $\nabla f \cdot \nabla g = (1/\varepsilon, 0) \cdot (0, 1/\varepsilon) = 0$.

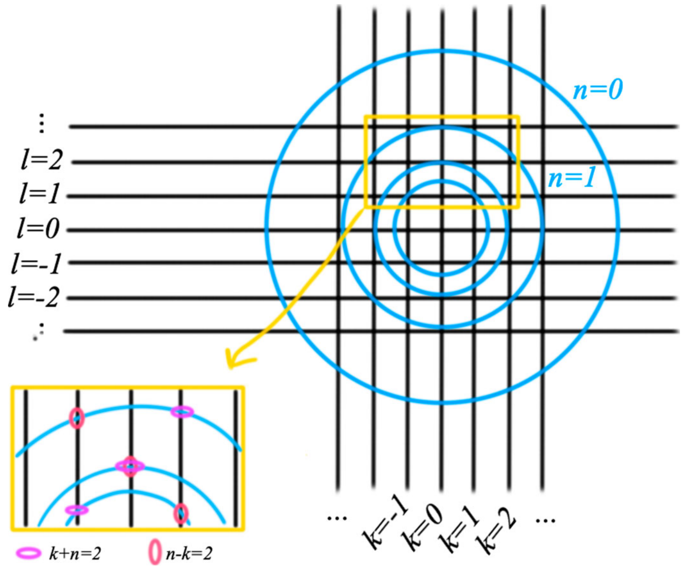

Figure 4. Gratings consisting of a Cartesian grid bounding 'pixels' and the concentric circles described in the text. The insert zooms and removes horizontal lines for better visualization, showing how series $n \pm k = \alpha$ are constructed.

- Patterns $n \pm k$, between circles and vertical lines, are visible when

$$\pm(1/\varepsilon, 0) \cdot \left(\frac{-2x}{T(x^2+y^2)^{3/2}}, \frac{-2y}{T(x^2+y^2)^{3/2}} \right) = \frac{\mp 2x}{T\varepsilon(x^2+y^2)^{3/2}} < 0 \iff \mp x > 0.$$

  Note that using the ℓ^p norm would give the same inequality.
- Likewise, patterns $n \pm l$ are visible when $\mp y > 0$.

In summary, the upper (resp. lower) half plane will comprise moiré patterns $n + l = \alpha$ (resp. $n - l = \alpha$), while the left (resp. right) half-plane will comprise moiré patterns $n - k = \alpha$ (resp. $n + k = \alpha$). In each quadrant, these patterns can interfere, whereas in regions of the form $x \approx 0$, $\pm y > 0$ or $y \approx 0$, $\pm x > 0$ only one type of pattern is expected. This is consistent with Figure 1 and more so still Figure 3, where hyperbolic patterns are more striking at the interfaces between quadrants.

The actual shape of the moiré patterns could be worked out using equations such as $n \pm k = \alpha$ in terms of x and y, using (7). However, this leads to implicit equations, which are not straightforward to interpret. Alternatively, an elegant approach for a closely related configuration has been previously presented (Cullen, 1990): regularly spaced gratings of straight lines and circles. Using geometric arguments and the polar definition of a conic, this previous work shows that moiré patterns are conics, whose eccentricity is given by the ratio between the pitches of the circular and linear gratings, respectively. Hence, if circles are closer to each other than lines one expects ellipses, whilst hyperbolas will occur when the lines are closer.

In our case, the distance between concentric circles is not a fixed quantity and the moiré patterns may not be perfect conics. Yet these previous results (Cullen, 1990) provide a useful heuristics, assuming some form of structural stability to the phenomenon: away from the origin, ε is small compared to the typical distance between circles, hence if the latter was constant one would expect hyperbolas (eccentricity > 1). As one approaches the origin, the distance between circles shrinks to zero and will necessarily become much lower than ε, however small the pixels may be, leading to ellipses as moiré shapes. This is confirmed in practice by our attempts at producing visual representations of surfaces of the form (2). For instance, Figure 1 comprises full circles at the periphery, where the pitch is too large to create any significant interference with the digitized display grid, then hyperbolic patterns which morph into ellipses as one approaches the origin. Eventually, the pixel size becomes large compared to the circles' typical pitch and moiré theory becomes ineffective.

Before presenting a series of figures based on the principles discussed thus far, we should point out that the gratings used in this section are only a model of what is actually happening. Indeed, rather that one-dimensional lines spanning the plane, pixels are two-dimensional items. The colour and/or light intensity which they bear is representative of neighbouring level curves, in a way which depends on the exact algorithm being used. This introduces some inherently two-dimensional features in any figure, which are ignored in the presentation above. Despite these limitations, the extensive literature on moiré patterns provides us with useful descriptive tools.

4. Sample of figures

In this section, we present a series of pictures created using the principles described above. We explore the effect of varying parameters such as the number of grid points (denoted n), the function S or its period T, the steepness exponent q, the norm ℓ^p. We also consider the effects of some of the many possible algorithms used for displaying the figures, in particular the choice of colour scheme and the anti-aliasing algorithm.

4.1. Perceptually uniform colour schemes

In this section, we rely only on colour schemes which are designed to be perceptually uniform (Hunter, 2007; Kovesi, 2015; van der Velden, 2020). As such, they give the closest representation of the surface map (2) itself, ignoring any aesthetic consideration. Below are a few figures, for different parameter choices.

First, we consider the effect of the grid resolution, controlled using the number of pixels denoted $n \times n$. From previous discussions, we expect conic like patterns to occur in a way which depends on the interplay between pixel size (inversely proportional to n) and the period T. We expect reducing the resolution (decreasing n) to have some similarity with increasing T. However, since the inter-circle distance varies non-linearly with T, see (5), we do not expect these two controls to be completely interchangeable. This is confirmed in Figure 5, where we see a similar, but not identical pattern when simultaneously doubling n and halving T. Other choices (not shown) confirm this principle. It is also generally the case that large values of n (or large T) lead to figures which are closer to the 'true' series of concentric circles, whilst smaller n or T leads to the occurrence of noticeable patterns. Below a certain limit of very small n or T, these patterns become less discernible as in the centre of Figures 1 or 5. See an example with period $T = 10^{-4}$ and $n = 800$ in Figure 6.

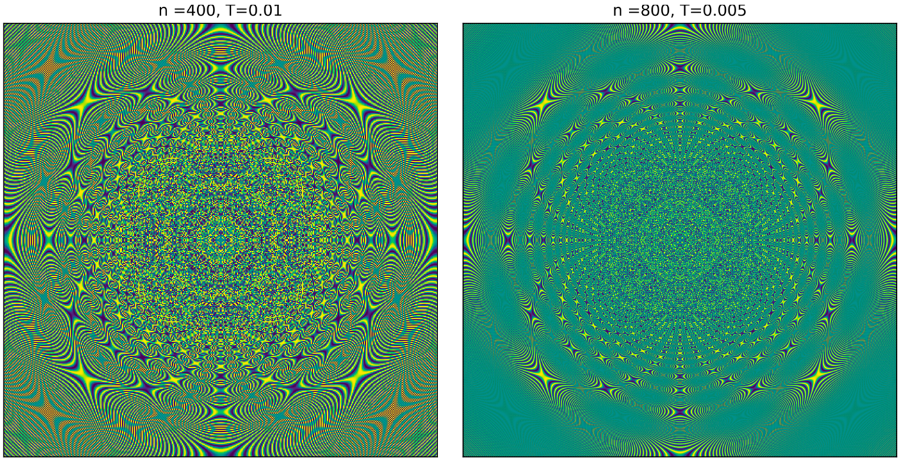

Figure 5. Heatmap of $S(1/(x^2+y^2))$, i.e. $q = 2$, with $S(x) = \frac{(1+\sin(2\pi x/T))}{2}$. The period T and grid size n are as shown above in each figure. The colourmap is `viridis`.

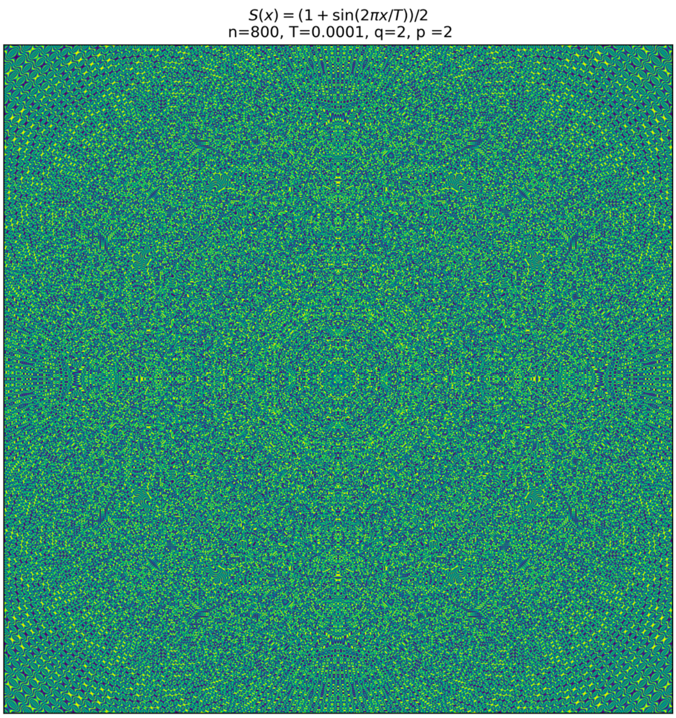

Figure 6. Heatmap of $S(1/(x^2+y^2))$, i.e. $q = 2$, with $S(x) = \frac{(1+\sin(2\pi x/T))}{2}$, $T = 0.0001$ and $n = 800$. The colourmap is `viridis`.

The parameters chosen for Figure 5 are in a range that yields striking patterns with a sinusoidal function S and $q = 2$. Figure 7 summarizes the main effects that can arise from varying S or q.

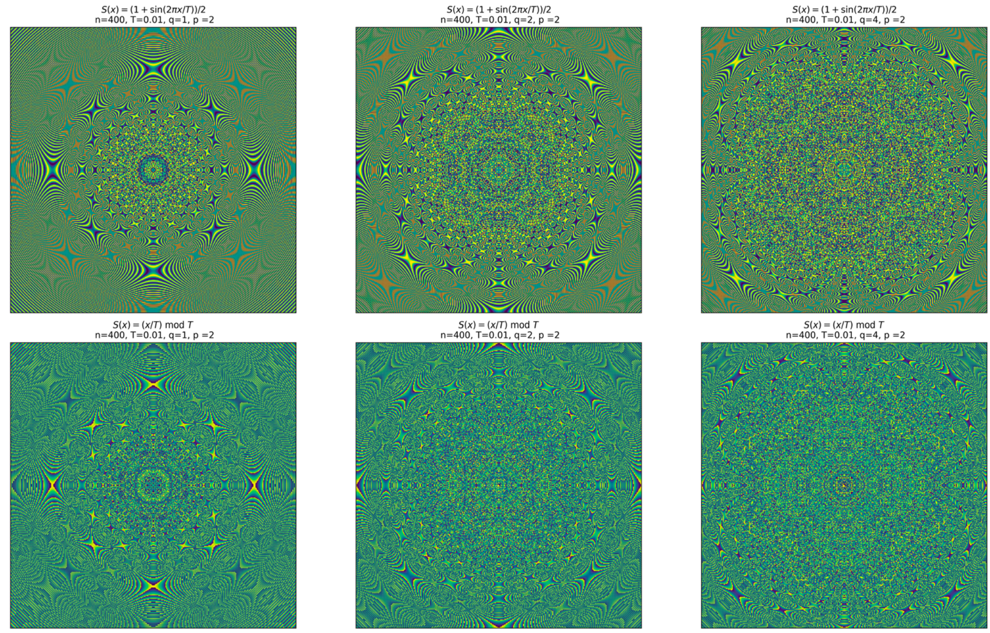

Figure 7. Heatmap of $S(1/(x^2+y^2)^{q/2})$ where S has period $T=0.01$ and $n=400$. Top row: S sinusoidal as in Figure 6, q as shown. Bottom row: S 'saw wave' as in Figure 6, q as shown. The colourmap is `viridis`.

The steepness parameter q has the dual effect of bringing circles closer together and adding a nonlinearity within each annular region $r \in I_n$. Departing from a sinusoidal S, the piecewise-linear 'saw wave' function S can be used to modulate the appearance of these patterns. As predicted in previous sections, the choice of S has an effect on the distribution of colours, but not on the overall geometry of the figure, which is determined by T and n. The discontinuity of the saw wave at multiples of T leads to sharper changes between the two extreme values of the colourmap, but this only of moderate impact, seeing how similar are the top and bottom rows of Figure 7. For this reason, in the following we will rely only on the sinusoidal S, since (i) we believe it yields slightly clearer patterns and (ii) it is widely available, as opposed to other periodic functions which would have to be implemented *de novo*.

Still using perceptually uniform colour schemes, additional patterns can appear as a result of the rendering algorithm. Indeed, any display method will have to rely on some form of interpolation of the data, to assign a colour value to each pixel; there are a variety of algorithms, see the documentation for the `imshow` command used throughout this paper (Hunter, 2007) .[1] In Figure 8, one illustrates this aspect by comparing two perceptually uniform colourmaps and two interpolation algorithms. We have selected two interpolation algorithms, known as the 'lanczos' and 'bicubic' methods. Both produce 'flower-like' patterns (particularly so with the `cet_rainbow4` colourmap Kovesi, 2015) which are thicker and smoother for the 'bicubic' method. The surprising amount of green visible on this figure is due to the nonlinearity of the interpolation method 'bicubic', which relies on cubic spline interpolation. This method is known to be accurate with finer details, but to

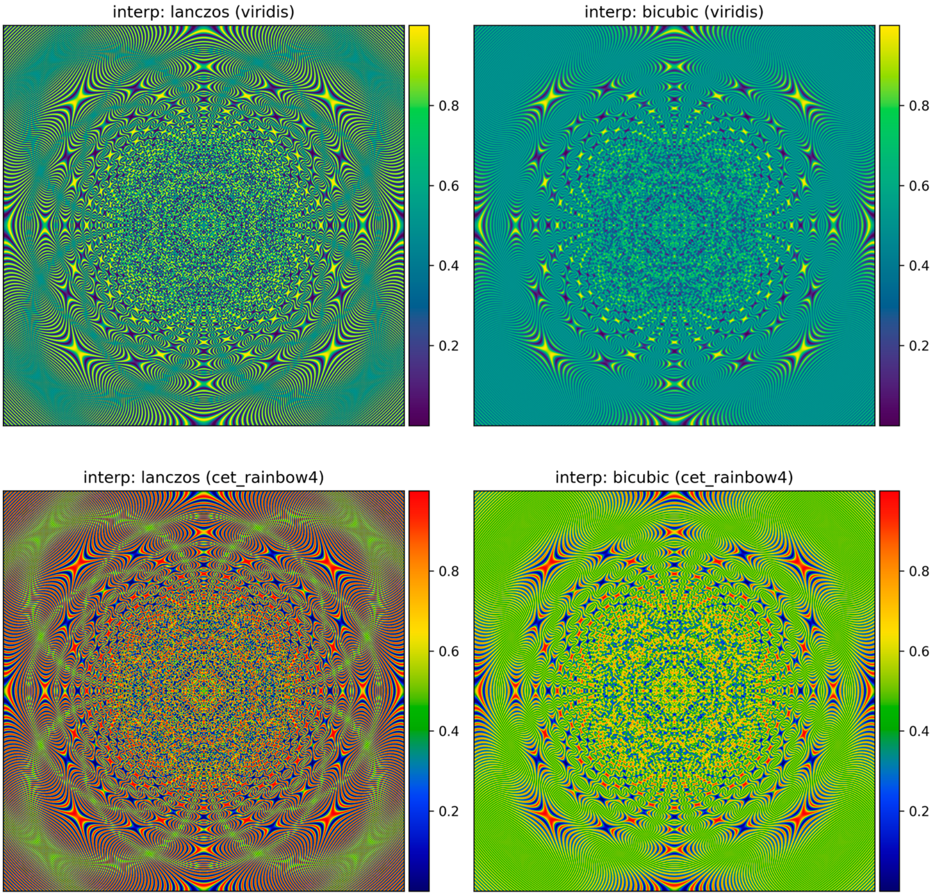

Figure 8. Heatmap of $S(1/(x^2 + y^2))$ where S is sinusoidal with period $T = 0.01$ and $n = 400$. Two colourmaps are compared and shown in the side of each panel. Two interpolation algorithms, known as the 'lanczos' and 'bicubic' methods, are used as shown above each panel.

induce artefacts otherwise. In the present context, this can be exploited for artistic aims. Other methods seem to produce variations where these structures are barely visible (see the default 'antialiasing' method in previous figures) or of intermediary thickness between the two shown in Figure 8.

4.2. Other colour schemes

As discussed earlier, it is equivalent to change the profile of the function S or the colour scheme being used in creating image. However, the latter is more practical since in most implementations one expect colourmaps to be available as a standard option, whereas designing complex periodic patterns require additional implementation. Given the very large number of available colourmaps in a library such as matplotlib, and combining this with different interpolation methods as discussed in the previous section, one can generate a myriad of figures based on a fixed choice of S, T, q and the resolution n. Combining the default colourmaps from matplotlib and those coming from well-documented libraries

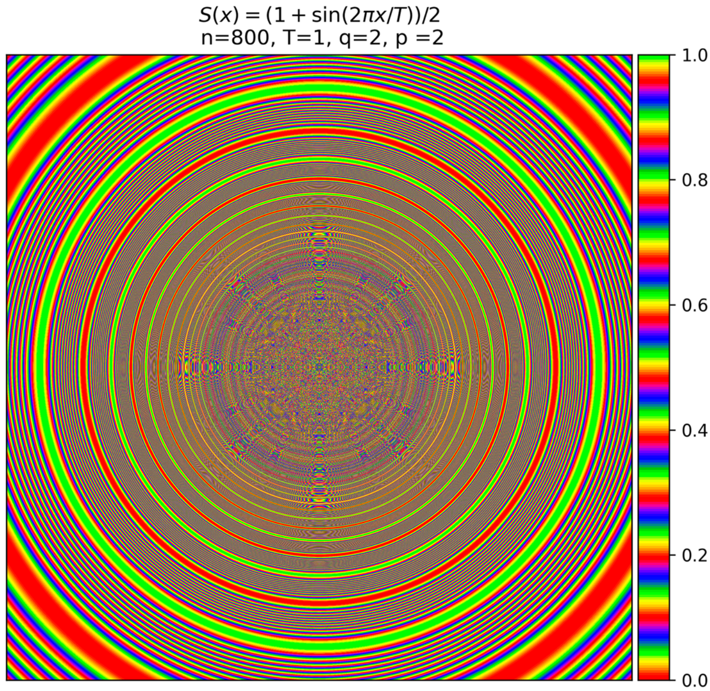

Figure 9. Heatmap of $S(1/(x^2 + y^2))$ where S is sinusoidal with period $T = 1$ and $n = 800$ and the short wavelength periodic colourmap `prism`. The 'bicubic' interpolation method is used.

cmasher (van der Velden, 2020) and colorcet (Kovesi, 2015) (which automatically get added to matplotlib's), one has over 700 colourmaps available. A striking example, using a colour scheme which is itself periodic with short period, is shown in Figure 9. We also show a small sample of the possible images that can be created with a unique choice of S and associated parameters in Figure 10, with more homogeneous colourmaps and two interpolation methods.

4.3. Interference patterns between ℓ^2 and ℓ^p norms

All figures seen so far are based on the ℓ^2 norm. However, much of the initial discussion remains largely valid if one were to use an alternative ℓ^p, with $p \neq 2$. In Figure 11, one can see some more patterns arising as p is varied. In particular, the nature of the conic-like patterns drastically changes at the critical value $p = 1$. As p becomes larger, square patterns dominate the figure as expected.

Since overall the patterns we have seen so far can all be described as resulting from an overlap between squares (the pixels) and circles, this led us to represent figures where both the Euclidean and ℓ^p norms are used, with patterns being superimposed. This was done by considering either the sum or product of two functions $f(r) = f(\|(x, y)\|_p)$ of the form (1), one with $p = 2$ and the other with $p \neq 2$. This resulted yet again in a new catalogue of striking geometric figures, of which a sample is shown in Figure 12. One particularity of these patterns is that they are most visible for larger values of the period T compared to previous figures.

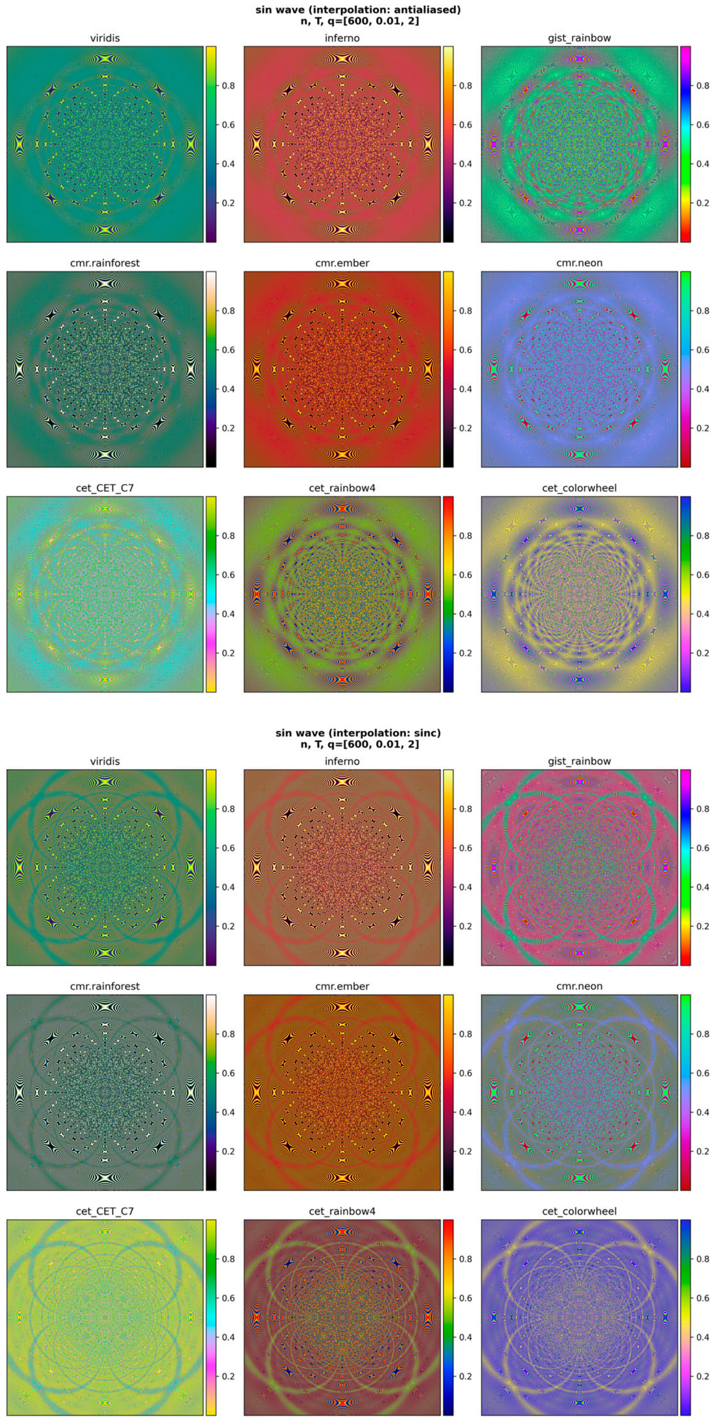

Figure 10. Heatmap of $S(1/(x^2+y^2))$ where S is sinusoidal with period $T=0.01$ and $n=600$. Nine colourmaps are compared and their names are shown above each panel. The 'antialiased' (resp. 'sinc') interpolation method is used on top (resp. bottom).

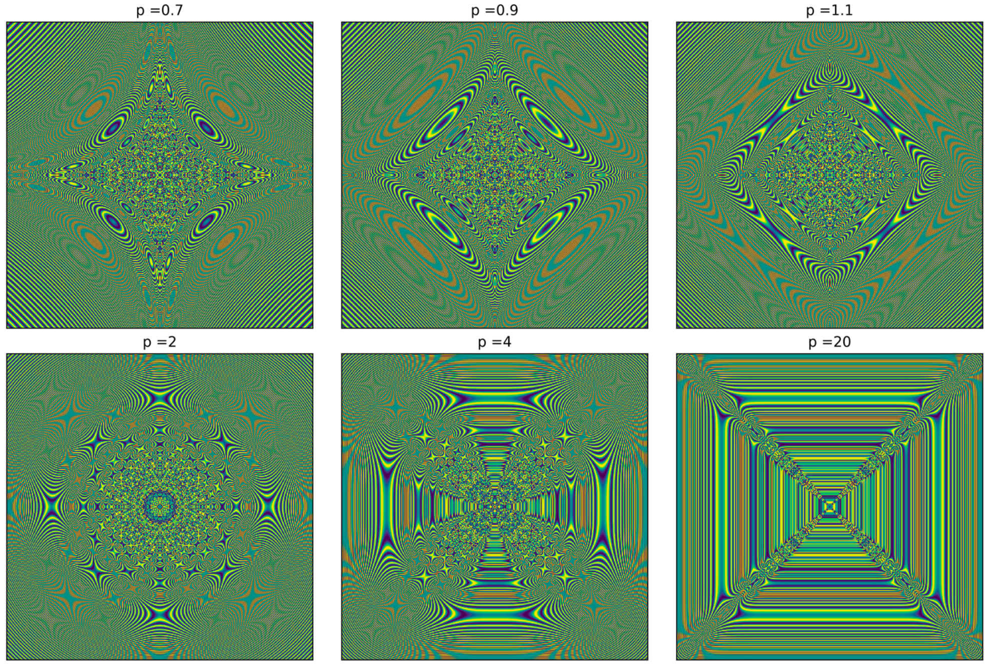

Figure 11. Heatmap of $S(1/\sqrt{x^2+y^2})$ where S is sinusoidal with period $T = 0.01$ and $n = 600$. Increasing values of the exponent p of the ℓ^p norm being used.

In Figure 12 as in previous images, a pleasant aesthetic experience results from the contrast between the large-scale interference of concentric patterns on the outer part of the figure, and the more intricate moiré patterns occurring at the centre. The chosen colourmap is reminiscent of patterns seen on stained glass in some gothic cathedrals.

5. Discussion

We have shown how a simple expression such as (2) is able to generate a variety of striking geometric figures. Their complex appearance results from the tension between the infinite nature of the object being represented and the necessary finiteness of any display medium. This was clearly identified in the previous literature (Kaplan, 2005) for very similar patterns, using a function whose frequency increases away from the origin instead of towards it and a gray-scale colourmap. In particular using the most widespread visualization device currently available, i.e. an electronic visual display, one observes interfering patterns resulting from the imperfect overlap between the square shape of pixels and the circles underlying the surface (2). It is not straightforward, in general, to guarantee that a computer generated plot is faithful to the mathematical object it represents (Melquiond, 2021). In the present context, the object is infinite and it is precisely by giving up on any attempt to be faithful that we can generate remarkable figures. A multitude of similar but unique patterns could be created by varying some of the parameters discussed in this note. To this effect, we provide a simple Jupyter notebook, which was used to create all figures in this paper and has been designed to allow for more patterns to be easily produced. This

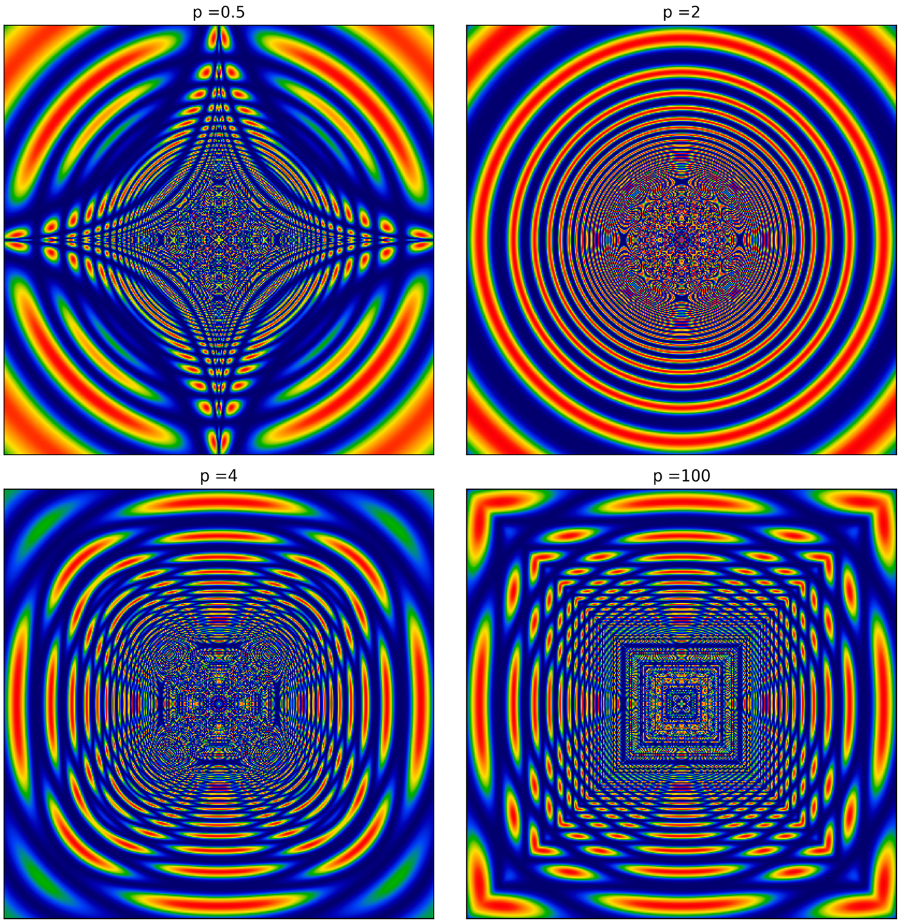

Figure 12. Heatmap of $S(1/(x^2+y^2)) \cdot S(1/(x^p+y^p)^{2/p})$ where S is sinusoidal with period $T=0.5$ and $n=800$. Increasing values of the exponent p of the ℓ^p norm being used.

includes animations where one or more of these parameters are varied by small increments within a range of values.

To include a speculative note, one may find it remarkable that the different figures we have presented are loosely reminiscent of archetypal patterns including mandalas (Jung, 1953) as well as hallucinatory figures (Blom, 2010; Klüver, 1942). Previous work has included algorithmic methods to create mandalas (Zhang et al., 2020). There are also a number of mathematical models describing hallucinations in mathematical neuroscience (Bressloff et al., 2001; Ermentrout & Cowan, 1979).

The present note does not allow us to bring any new argument about any mechanism underlying the prevalence of such patterns in human artistic and mental productions. However, it provides a very simple and concise mathematical device which allows to generate a vast array of attractive figures. One may notice in passing that the function $A\sin(1/r)+B\cos(1/r)$ (for arbitrary constants A, B) is a general solution to the differential equation

$$r^4u'' + 2r^3u' + u = 0.$$

Although this differs dramatically from equations featured in the references above, one may wonder whether this form, or another admitting solutions of the form (1), may arise as models of the brain activity in some specific circumstances.

To conclude, let us put aside these hypothetical speculations, and hope that the reader will have found the figures shown above as enjoyable to contemplate as it has been to produce them.

Note

1. Also https://matplotlib.org/stable/gallery/images_contours_and_fields/interpolation_methods.html (accessed Jan. 2025).

Acknowledgments

The author would like an anonymous reviewer for pointing to reference Kaplan (2005), which discusses patterns having much in common with those seen here.

Disclosure statement

No potential conflict of interest was reported by the author(s).

ORCID

E. Farcot http://orcid.org/0000-0002-0742-3028

References

Amidror, I. (2009). *The theory of the moiré phenomenon. Volume 1: Periodic layers*. Springer.
Blinn, J. (1987). How many ways can you draw a circle? *IEEE Computer Graphics and Applications*, *7*(8), 39–44. https://doi.org/10.1109/MCG.1987.276918
Blom, J. D. (2010). *A dictionary of hallucinations*. Springer.
Bressloff, P. C., Cowan, J. D., Golubitsky, M., Thomas, P. J., & Wiener, M. C. (2001). Geometric visual hallucinations, Euclidean symmetry and the functional architecture of striate cortex. *Philosophical Transactions of the Royal Society of London. Series B: Biological Sciences*, *356*(1407), 299–330. https://doi.org/10.1098/rstb.2000.0769
Cullen, M. R. (1990). Moiré fringes and the conic sections. *The College Mathematics Journal*, *21*(5), 370–378.
Ermentrout, G. B., & Cowan, J. D. (1979). A mathematical theory of visual hallucination patterns. *Biological Cybernetics*, *34*(3), 137–150. https://doi.org/10.1007/BF00336965
Foley, J. D., van Dam, A., Feiner, S. K., & Hughes, J. (1995). *Computer graphics: Principles and practice*. Addison-Wesley.
Hunter, J. D. (2007). Matplotlib: A 2D graphics environment. *Computing in Science & Engineering*, *9*(3), 90–95. https://doi.org/10.1109/MCSE.2007.55
Jung, C. G. (1953). *Mandala symbolism: Collected works* (Vol. 12. Psychology and alchemy). Pantheon Books.
Kaplan, C. S. (2005). Aliasing artifacts and accidental algorithmic art. In *Renaissance Banff: Mathematics, music, art, culture* (pp. 349–356). Canadian Mathematical Society.
Klüver, H. (1942). Mechanisms of hallucinations. In Q. McNemar & M. A. Merrill (Eds.), *Studies in personality* (pp. 175–207). McGraw-Hill.
Kovesi, P. (2015). *Good colormaps: How to design them*. Preprint arXiv:1509.03700
Melquiond, G. (2021). *Plotting in a formally verified way*. Preprint arXiv:2108.03974
Theocaris, P. S. (1969). *Moiré fringes in strain analysis*. Pergamon.

van der Velden, E. (2020). *CMasher: Scientific colormaps for making accessible, informative and 'cmashing' plots*. Preprint arXiv:2003.01069

Zhang, J., Zhang, K., Peng, R., & Yu, J. (2020). Parametric modeling and generation of Mandala Thangka patterns. *Journal of Computer Languages*, *58*, 100968. https://doi.org/10.1016/j.cola.2020.100968